Journal of Sol-Gel Science and Technology
https://doi.org/10.1007/s10971-019-04956-x

ORIGINAL PAPER: NANO-STRUCTURED MATERIALS (PARTICLES, FIBERS, COLLOIDS, COMPOSITES, ETC.)

Check for updates

The effect of Zr loading in Zr/TiO_2 prepared by pressurized hot water on its surface, morphological and photocatalytic properties

Jaroslav Lang[1] · Lenka Matějová[1] · Zdeněk Matěj[2] · Libor Čapek[3] · Alexandr Martaus[1] · Martin Kormunda[4]

Received: 12 December 2018 / Accepted: 1 March 2019

Abstract

Zr/TiO_2 anatase photocatalysts with 0.5, 1, 2, 5 and 7.5 mol.% Zr were prepared using pressurized hot water crystallization and their photocatalytic activity was explored in acid orange 7 photodegradation. Parent TiO_2 was also prepared and tested. From all tested photocatalysts, 2 mol.% Zr/TiO_2 showed the highest photoactivity, and 7.5 mol.% Zr/TiO_2 showed the lowest photoactivity. The poor photoactivity of 7.5 mol.% Zr/TiO_2 can be explained by the amorphous ZrO_2 present in the surface layer (~1–3 μm depth) of TiO_2 anatase nanocrystallite agregates which changed the aggregate morphology and shielded the anatase nanocrystallite surface. The type and amount of defects (e.g., oxygen vacancies, lattice defects) did not effect the photoactivity of Zr/TiO_2 in AO7 photodegradation. The addition of Zr to TiO_2 significantly affects the photocatalyst morphology and the location where amorphous ZrO_2 forms. The optimal Zr loading in TiO_2 was determined to be 2 mol.%.

Graphical Abstract

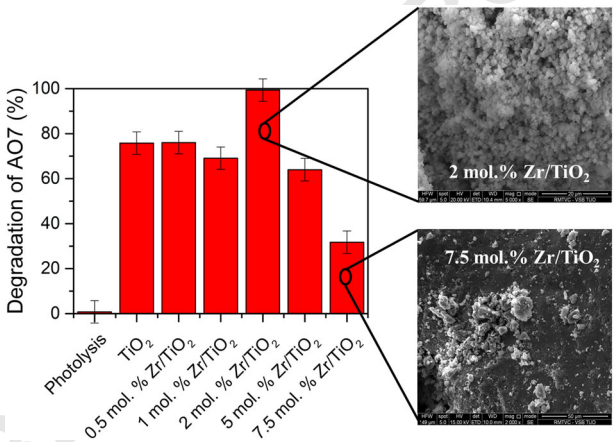

Supplementary information The online version of this article (https://doi.org/10.1007/s10971-019-04956-x) contains supplementary material, which is available to authorized users.

✉ Jaroslav Lang
jaroslav.lang@vsb.cz

[1] Institute of Environmental Technology, VŠB–Technical University of Ostrava, 17. listopadu 15/2172, 708 00 Ostrava-Poruba, Czech Republic

[2] MAX IV Laboratory, Lund University, Fotongatan 2, 225 92 Lund, Sweden

[3] Department of Physical Chemistry, Faculty of Chemical Technology, University of Pardubice, Studentská 573, 532 10 Pardubice, Czech Republic

[4] Department of Physics, Faculty of Science, Jan Evangelista Purkyně University, Pasteurova 1, 400 96 Ústí nad Labem, Czech Republic

Keywords Subcritical water · Pressurized hot water crystallization · Zirconium; Titanium dioxide · Photocatalysis

1 Introduction

The pollution produced during processing and use of fuels affects the environment on a global scale. The anthropogenic man-made pollution was linked to the depletion of the ozone layer, greenhouse effect and global warming. There is a global initiative to lower the emissions and amounts of pollutants now [1].

Photocatalysis is already applied to pollution abatement [2, 3]. Most notable are semiconductor photocatalysts like ZnO [4–6], TiO_2 [3, 7–9] and g-C_3N_4 [10–13]. Semiconductor photocatalysts utilize energy supplied by photons to create electron–hole pairs used in chemical processes. These chemical processes may be applied to abate air and water pollution. The advantage of the photocatalysts is that the energy is supplied via light (possibly daylight) and their reusability. However, most of the photocatalysts require ultraviolet (UV) light for their proper function. This UV light is represented in the daylight spectrum by only 4%. Therefore, the current challenge for the researchers is to develop photocatalysts that are more effective or utilize bigger part of the daylight spectrum.

One of the most researched photocatalyst materials is TiO_2. The TiO_2 is often doped with other elements to improve visible light absorption and improve photocatalytic performance [7, 14–16]. The Ti and Zr are transitional metals from IVb group of elements and their oxides TiO_2 and ZrO_2 show similar physico-chemical properties. ZrO_2 has larger band gap than TiO_2; in fact, both the valence band and conduction band of TiO_2 energetically lie within the ZrO_2 band gap [17]. The ZrO_2 possibly acts as trap for holes and electrons and delays their recombination [18]. The electrons are trapped on the ZrO_2. Prolonged lifetime of the electron–hole pair increases their chances to undergo desired interaction with adsorbed pollutant or creation of radicals [19]. The Zr doped TiO_2 also benefits from increased thermal stability of the TiO_2 phases [20], surface acidity and surface area [21]. The benefits of Zr dopation to TiO_2 on photocatalytic decomposition of pollutants were studied for a number of chemicals, e.g., Ibuprofen [22], Bisphenol A [23], acetonitrile in a gas phase [24], 4-chlorophenol [19], 4-nitrophenol [25], 2-chloroethyl ethyl sulfide and dimethyl methylphosphonate [26], formic acid [27], nitric oxide [28], Rhodamine B [29, 30], volatile organic compounds [31], phenol [32] and toluene [33]. Acid orange 7 (also known as Orange II or Egacide orange) represents monoazo dyes. It is used in textile and cosmetic industry and as a consequence can be found in waste water [34]. Its photocatalytic degradation is very well covered in literature [35].

This work continues the study of Zr doped TiO_2 materials crystallized using pressurized hot water for use in the photocatalysis. Previous work reported on the topic of $Zr_xTi_{x-1}O_n$ mixed oxides (the Zr content was much higher and ranged from 10 to 90 mol.%) and it was concluded that the optimal Zr content for photocatalytic purposes of Zr doped TiO_2 materials is below 10 mol.% of Zr [36]. The optimal crystallization conditions for pressurized hot water processing were found to be the temperature of 250 °C, pressure of 10 MPa and 2 L of water [37]. Thus, a set of low Zr loading doped TiO_2 was prepared using optimal processing/crystallization conditions and its photocatalytic properties in AO7 photodegradation were investigated in the current study. Additionally, the electrochemical and photoluminescence measurements were carried out to look into the phenomena taking place on the surface of prepared photocatalyst, affecting their photoactivity. The surface composition and Zr/TiO_2 morphology was also examined in detail.

2 Experimental

2.1 Preparation of materials

The Zr/TiO_2 materials were synthetized by thermal hydrolysis from the solution of titanyl sulfate ($TiOSO_4$) and zirconium oxynitrate ($ZrO(NO_3)_2$) and sulfuric acid. The precipitate was neutralized, washed with demineralized water and dried. The acquired powder Zr/TiO_2 materials were crystallized using pressurized hot water processing. Five Zr/TiO_2 oxides were synthetized; the Zirconium content was calculated to 0.5, 1, 2, 5 and 7.5 mol.%, respectively. The typical synthesis is shown on the 0.5 mol.% Zr/TiO_2.

The 0.5 mol.% Zr/TiO_2 was prepared as follows: 0.0848 g $ZrO(NO_3)_2.6\ H_2O$ was dissolved under vigorous stirring (300 rpm) in 453 mL of 0.5 wt.% sulfuric acid and mixed with 47 mL of titanyl sulfate solution (100 g TiO_2/1 L). The amount of dilute sulfuric acid was calculated and so the mixture with titanyl sulfate solution had volume of 0.5 L. This colloid solution was heated up to 100 °C. After the precipitation began, the temperature was lowered and kept at 90 °C for 1 h. The mixture was cooled down and neutralized with 29 mL of 20 wt.% NaOH solution. The precipitate was filtered and washed with demineralized water.

The supernatant was tested with the $BaCl_2$ for the presence of sulfate anions. The sulfates were washed out with 3 L of demineralized water and the sulfate test was negative. Filter cake was dried at 50 °C overnight. The dried filter cake was then crystallized using pressurized hot water processing. The powderized filter cake sieved to <0.160 mm particle-size fraction was loaded into a 24 mL high-temperature stainless steel cell and placed in an oven with rapid heating. The inlet on the bottom of the steel cell was connected by steel capillary to the gradient pump. The upper outlet of the steel cell was connected to steel capillary submerged in a cooling water bath. The pressure was regulated by changing of the length and diameter of polyether ether ketone capillaries connected to the outlet steel capillary. The processing conditions were $T = 250$ °C and $p = 10$ MPa and the amount of water pumped through the cell was 2 L of water. For further information regarding synthesis and processing, please refer to refs. [36, 37]. The scheme of apparatus for pressurized hot water processing is shown in ref. [38].

2.2 Characterization of materials

The structural properties (phase composition) and microstructural properties (volume-weighted crystallite size, lattice parameters) of powder Zr/TiO_2, ZrO_2 and TiO_2 were determined using powder X-ray diffraction (XRD). XRD patterns were obtained using a Rigaku SmartLab diffractometer (Rigaku, Japan) with detector D/teX Ultra 250. The X-ray source was cobalt lamp (CoKα, $\lambda = 0.17889$ nm). The powder materials were pressed in carousel holder and measured in the reflection mode. The XRD patterns were collected in a 2Θ range from 5° to 90° with a step of 0.01° and speed 0.5 °/min. Diffraction patterns were analyzed with the aid of MStruct [39], the powder diffraction software which is based on the Rietveld method with several extensions for nanocrystalline materials [40]. XRD quantitative phase analysis was performed via the Rietveld method and assuming following phases: TiO_2 anatase, brookite, rutile, ZrO_2 tetragonal and monoclinic.

X-ray fluorescence spectrometry (XRF) was measured on an ARL 9400 XP sequential WD-XRF spectrometer in order to determine the chemical composition of all prepared powder materials. All peak intensity data were collected under the air atmosphere. The spectrometer uses four different targets in order to adjust the incident radiation for given group of elements. The excitation condition and the time of data collection were the following: Al-target (49 kV/0.7 mA/300 s), Mo-target (40 kV/0.44 mA/300 s), Co-target (35 kV/1 mA/300 s) and HOPG-target (17 kV/1.5 mA/300 s).

Textural properties of powder materials were studied using nitrogen physisorption measurement at −198 °C. The measurement was performed using a 3-Flex Micromeritics instrument. Prior to the nitrogen adsorption–desorption measurements, the materials were degassed at temperature 150 °C for 24 h under vacuum lower than 1 Pa to remove physisorbed water. The specific surface area was calculated according to the Brunauer–Emmett–Teller (BET) theory for the p/p_0 range 0.05–0.25 and marked as S_{BET} (in m^2/g) [41, 42]. The net pore volume, V_{net}, was determined from the nitrogen adsorption isotherm at relative pressure p/p_0 ~0.990.

Ultraviolet–visible (UV–vis) diffuse reflectance spectra of hydrated and granulated materials were measured in quartz cuvettes using a GBS CINTRA 303 spectrometer equipped with a Spectralon-coated integrating sphere. The spectra were recorded in the 200–800 nm wavelength range with the lamp switched at 350 nm. The reflectances were re-calculated to the absorption using the Schuster–Kubelka–Munk equation, $F(R\infty) = (1 - R\infty)^2/2\,R\infty$, where $R\infty$ is the diffuse reflectance from a semi-infinite layer. The obtained spectra were transformed to the dependencies $(F(R\infty) \times hv)^2$ against h. Kubelka–Munk function was used to estimate the band gap energy of the prepared materials. As both TiO_2 and ZrO_2 are indirect semiconductors, the indirect band gap energy was also determined by extrapolation of the linear part of curve $(F(R)^{1/2} = 0$.

Transmission electron microscopy (TEM) analysis was measured on a JEOL 2100 microscope at 200 kV of accelerating voltage. Prior to analysis, purified and ultrasonified water for 3 min was added to powder material placed in small Eppendorf tube. Suspensions were dropped on a copper grid with porous carbon film and dried on air.

Photoelectrochemical measurements were determined in three-electrode setup. One electrode constituted of photocatalyst powder deposited onto indium-tin oxide (ITO) foil coated by polyethylene terephthalate film. The Pt wire served as counter electrode and Ag/AgCl electrode was used as the reference electrode. The 0.1 M KNO_3 was used as an electrolyte solution. The electrolyte in the measuring cell was 15 min prior to and during measurement purged by argon to eliminate any dissolved oxygen. The light source was 150 W Xe lamp. The induced photocurrent was recorded using a photoelectric spectrometer coupled with the P-1F 1.6 potentiostat (Instytut Fotonowy, Poland). The photocurrent spectra were recorded within range of 240–500 nm with the step of 10 nm in the potential range of −0.2 to 0.7 V, step 0.1 V.

Photoluminescence (PL) spectra were measured by a FLS920 spectrometer (Edinburgh Instrument Ltd, UK). The spectrometer was equipped with a 450 W Xenon lamp (Xe900). The excitation wavelength was 325 and 386 nm. The width of excitation and emission slits was 3 nm and spectra were measured in the range from 250 to 630 nm (resp. 530 nm).

The surface composition of the materials and the chemical states of the elements were inspected by X-ray

Table 1 Chemical composition, textural and optical properties of prepared Zr/TiO_2 oxides

Material	XRF		Nitrogen physisorption			DRS	
	TiO_2 (wt.%)	ZrO_2 (wt.%)	Porous character	S_{BET} (m^2/g)	V_{net} (mm^3_{liq}/g)	Direct E_g (eV)	Indirect E_g (eV)
0.5 mol.% Zr/TiO_2	99	1	Macro-mesoporous	99	297	3.36	3.08
1 mol.% Zr/TiO_2	98	2	Macro-mesoporous	100	324	3.38	3.14
2 mol.% Zr/TiO_2	97	3	Macro-mesoporous	91	291	3.39	3.13
5 mol.% Zr/TiO_2	93	7	Macro-mesoporous	89	378	3.38	3.11
7.5 mol.% Zr/TiO_2	90	10	Macro-mesoporous	83	360	3.32	3.02
TiO_2 [36]	100	0	Mesoporous	117	271	–	3.11

XRF X-ray fluorescence spectrometry, *DRS* diffuse reflectance spectroscopy

photoelectron spectroscopy (XPS) using a SPECS PHOIBOS 100 hemispherical analyzer with a 5-channel detector and a SPECS XR50 X-ray source equipped with an Al and Mg dual anode. The measurements were performed with Al anode at Epass 40 eV for survey spectra and Epass 10 eV for high-resolution spectra. The acquired data were processed in CasaXPS software with Shirley background profile and built-in RSF were used for calculation of the compositions from high-resolution spectra.

The scanning electron microscope (SEM) Quanta FEG 450 (FEI, Czech Republic) with energy-dispersive spectrometer OCTANE (EDS, USA) was used for characterization of the morphology of the studied samples and surface elemental composition. Images were taken using secondary and backscattered electron detectors at 15–20 keV.

2.3 The photoactivity test

The photoactivity was determined using azo-dye Acid orange 7 photodegradation. The powder photocatalyst was mixed with the solution of azo-dye and the resulting suspension was illuminated with UV light. The changes to the dye concentration due to photoactivity of the photocatalyst were determined from the changes in absorbance of the dye solution.

The powder photocatalyst (0.05 g) was mixed with 150 mL of Acid orange 7 solution ($c = 3.10^{-5}$ mol/L). The resulting suspension was kept stirring (400 rpm) in dark for 30 min. After 30 min in the dark, the absorbance value was measured and UV illumination started. The UV light was from Narva Blacklight blue lamp ($\lambda = 365$ nm, 36 W) and sampling was realized at first in 30 min and later in 60 min intervals. The samples were taken with syringe (2 mL of the suspension was taken) and filtered (syringe filter with 0.45 μm pore size with the glass prefilter). One milliliter of the filtered solution was diluted with demineralized water to 10 mL solution and the absorption was measured on this dilute solution. The calibration curve was determined using different concentrations of AO7 solution (0, 0.6, 1.2, 2.4 and 6.10^{-5} mol/L). The regression curve from calibration data had following equation: $y = 16{,}766x + 0.0049$, $R^2 = 0.9998$.

The decrease of the dye concentration due to photoactivity of the photocatalyst was determined using UV–vis spectrometer Specord 250 Plus with software WinASPECT PLUS version 4.1.0.0.

3 Results and discussion

3.1 Characterization of materials

The Zr/TiO_2 oxides were synthetized using thermal hydrolysis and crystallized using pressurized hot water. The crystallization conditions were: 250 °C, 10 MPa, 2 L of water. The Zr/TiO_2 oxides were characterized with the following methods: XRF, nitrogen physisorption measurement, UV–vis diffuse reflectance spectroscopy (DRS), XRD, TEM analysis, photocurrent measurement and PL spectroscopy. The photocatalytic activity was tested with Acid orange 7 degradation test. The processed materials are designated as x mol.% Zr/TiO_2, where x is the Zr molar content ranging from 0.5 to 7.5%. For further details regarding the pressurized hot water crystallization, please refer to refs. [36, 37].

The effect of pressurized hot water processing on (micro) structure, textural, optical, electronic and photocatalytic properties of prepared Zr/TiO_2 oxides on AO7 photodegradation was examined.

The chemical composition, textural and optical properties of processed Zr/TiO_2 oxides are summarized in Table 1.

The calculated and measured chemical composition is in good agreement. The synthesized Zr/TiO_2 oxides are macro-mesoporous solids with surface areas ~80–100 m^2/g, and the specific surface area decreases with the increasing Zr content in TiO_2. The decreased specific surface area of Zr/TiO_2 oxides can be attributed to larger TiO_2 anatase crystallite size (growing from 13.4 nm in 0.5 mol.% Zr/TiO_2 up to 16 nm in 7.5 mol.% Zr/TiO_2) (Table 2). According to XRD patterns (Fig. 1) all prepared crystalline Zr/TiO_2

Table 2 Phase composition and microstructure of prepared Zr/TiO_2 oxides

Material	Phase composition	$<D>_V$ (nm)	Lattice parameters	
			a (Å)	*c* (Å)
0.5 mol.% Zr/TiO_2	Anatase	13.4	3.786	9.501
1 mol.% Zr/TiO_2	Anatase	13.8	3.787	9.506
2 mol.% Zr/TiO_2	Anatase	14.4	3.788	9.518
5 mol.% Zr/TiO_2	Anatase	16.0	3.792	9.546
7.5 mol.% Zr/TiO_2	Anatase	16.0	3.796	9.565
TiO_2 [36]	96 wt.% anatase, 4 wt.% brookite	11.2[a]	3.789[a]	9.506[a]

$<D>_V$ volume-weighted crystallite size

[a]Anatase phase

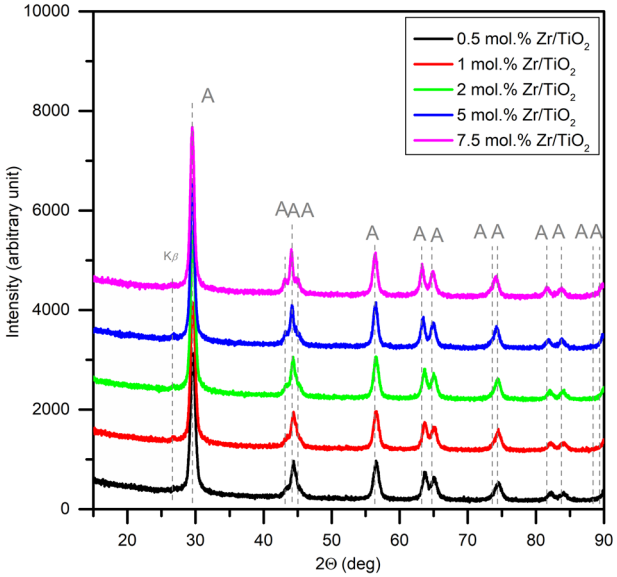

Fig. 1 X-ray powder diffraction (XRD) patterns of Zr/TiO_2 oxides. A, TiO_2 anatase

oxides are composed solely of anatase crystal phase. No other crystallographic phases like brookite, rutile, ZrO_2 tetragonal and monoclinic were detected. The Zr content (0.5–7.5 mol.% Zr) is so low that the Zr does not form a separate ZrO_2 crystal phases and serves as a dopant in TiO_2. This feature can be seen from the anatase lattice parameters (Table 2). The incorporation of Zr^{4+} into TiO_2 anatase crystal lattice (for Ti^{4+}) is taking place. The ionic radius of Zr^{4+} ions (0.59 Å) is larger compared to ionic radius of Ti^{4+} ions (0.42 Å) [43]. The difference in ionic radius of substituent Zr^{4+} causes elongation of the anatase crystal cell which can be seen as an increase of the *c* anatase lattice parameter as mentioned in ref. [37]. The progressive increase of *c* anatase lattice parameter corresponds well with the increasing Zr loading in the set (Table 2).

The optical results evaluated from DRS UV–vis measurements (Table 1) show a marginal increase in direct and indirect E_g with the increase of Zr content (from 3.08 to 3.14 eV). The 7.5 mol.% Zr/TiO_2 oxide shows drop in the E_g (to 3.02 eV).

The TEM images of 2 mol.% Zr/TiO_2 in Fig. 2a, b prove crystalline material. From the histogram in Fig. 3 the narrow crystallite size distribution with maximum crystallite size between 10 and 15 nm is apparent. These results are in a good agreement with the ~13–16 nm crystallite size determined from XRD (Table 2).

The photoelectrochemical measurement in Fig. 4 was used to assess and predict the photocatalytic activity of the prepared Zr/TiO_2 oxides. All of the oxides showed photogenerated current under irradiation with the wavelengths λ = 320 nm and higher (Fig. 4a). Figure 4b shows the photocurrent measured at λ = 360 nm (the closest wavelength corresponding to the maximum of the lamp used in photocatalytic experiment). In all of the measured oxides, a slow recombination (apparent from the shoulder on the right side at the base of the peak) is apparent. Initial fast rise followed by slower rise to a steady-state value is probably caused by imbalance in charge carriers mobilities (electrons and holes). The fast rise can be attributed to the faster carrier and a subsequent slow rise to the slower carrier [44]. The photocurrent responses were recorded at applied external potential of 0.7 V. When external potential is applied to the ITO foil (working electrode), the generated electrons are forced to transfer from the photocatalyst to the ITO, preventing them to recombine with holes. Such a result gives information about the amount of generated charge carriers which was the highest for 0.5 mol.% Zr/TiO_2 (Fig. 4b). However, higher amount of charge carriers does not mean higher photocatalytic activity which is seen from the photocatalytic results (discussed later in the section 'Photocatalytic results') where the most photocatalytically active photocatalyst (2 mol.% Zr/TiO_2) had the lowest photocurrent at 360 nm (Fig. 4b). These results are pointing toward a significantly more effective separation of charge carriers in this photocatalyst compared to the other four, which is the goal of this work, to find optimal loading of zirconium to lower the recombination rate of charge carriers as much as possible.

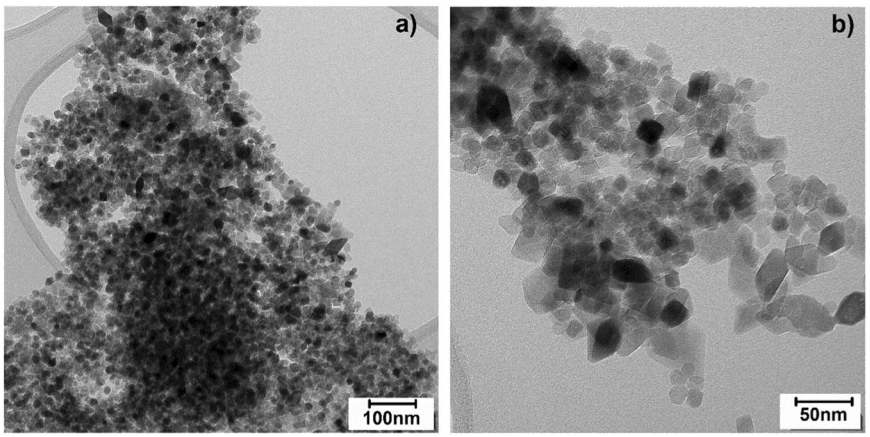

Fig. 2 The transmission electron microscopy (TEM) images of 2 mol.% Zr/TiO_2

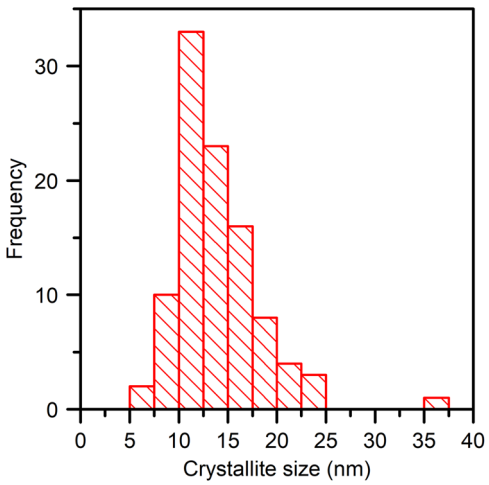

Fig. 3 Crystallite size distribution of 2 mol.% Zr/TiO_2 determined from transmission electron microscopy (TEM) image

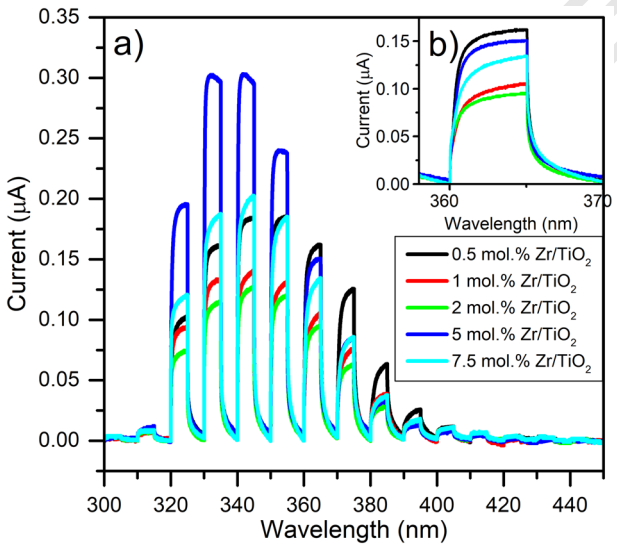

Fig. 4 **a** The photoelectrochemical measurement of Zr/TiO_2 oxides. **b** The detail of the photoelectrochemical measurement of Zr/TiO_2 oxides at 360 nm

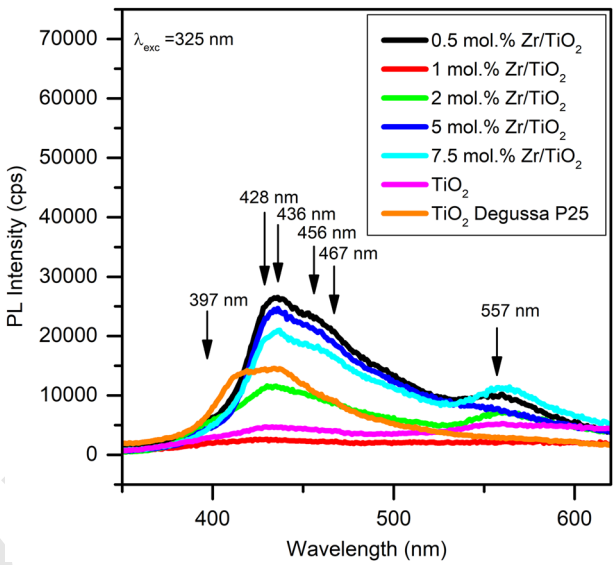

Fig. 5 The emission spectra of Zr/TiO_2 oxides

In Fig. 5 the emission spectra of selected Zr/TiO_2 oxides are shown and for comparison parent TiO_2 and TiO_2 Degussa P25 are added. On the basis of shape and intensity of the gathered spectra, three groups/types of PL spectra can be distinguished. The high intensity of emission peak indicates large amount of structural defects of similar type. The first group consists of 0.5 mol.% Zr/TiO_2, 5 mol.% Zr/TiO_2, 7.5 mol.% Zr/TiO_2 and 2 mol.% Zr/TiO_2 with peaks at 428, 456 and 557 nm and high PL intensity. TiO_2 Degussa P25 with characteristic peaks at 411 and 437 nm belongs to the second group, and its spectrum has lower intensity than the first group of materials. The third group consists of TiO_2 and 1 mol.% Zr/TiO_2. The spectra in the third group have very low intensity and only hints of peaks at 428, 456 and 557 nm.

From comparison of peak intensities at 557 nm, it can be assumed that the significant increase in PL intensity of Zr/TiO_2 oxides is due to the Zr dopation. The large emission band from 350 to 530 nm can be divided into two bands.

Table 3 The surface elementary composition of Zr/TiO_2 determined by X-ray photoelectron spectroscopy

Material	Concentration [atm.%]				Ratio O/Ti	Amount in [%]			
	C1s	O1s	Ti2p	Zr3d		O1s O-metal	O1s -OH	TiO_2	Sum of subTiO
0.5 mol.% Zr/TiO_2	10.9	61.8	27	~0.3	2.3	95	5	97	3
1 mol.% Zr/TiO_2	6.4	64.9	28.2	~0.5	2.3	95	5	95	5
2 mol.% Zr/TiO_2	16.5	58.8	24	~0.8	2.5	93	7	96	4
5 mol.% Zr/TiO_2	12.4	61.9	23.8	2	2.6	91	9	95	5
7.5 mol.% Zr/TiO_2	10.8	61.6	23.9	3.6	2.6	93	7	93	7
TiO_2	9.5	64.5	26	0	2.5	91	9	96	4

'~' Means rough estimation based on X-ray photoelectron spectroscopy (XPS) measurements

Table 4 The comparison of Zr/Ti atomic ratios determined by different techniques

Material	Theoretical	XRF	SEM-EDS[a]	XPS
	Zr/Ti ratio	Zr/Ti ratio	Zr/Ti ratio	Zr/Ti ratio
0.5 mol.% Zr/TiO_2	0.0050	0.0065	0.0038	~0.0111
1 mol.% Zr/TiO_2	0.0101	0.0132	n.d.	~0.0177
2 mol.% Zr/TiO_2	0.0204	0.0201	0.0148	~0.0333
5 mol.% Zr/TiO_2	0.0526	0.0488	n.d.	0.0840
7.5 mol.% Zr/TiO_2	0.0811	0.0720	0.0743	0.1506
TiO_2	–	–	–	–

SEM-EDS scanning electron microscope–energy-dispersive spectrometer, *XPS* X-ray photoelectron spectroscopy, *n.d.* not detected, '~' means rough estimation based on XPS measurements

[a]The atomic % of Zr and Ti was determined from the 1 μm^2 area of the material surface as an average value taken from 4 different places within the material surface

One from 400 to 442 nm can be attributed to self-trapped excitons [45] and the second one from 442 to 561 nm to shallow trap levels at 456, 467, 490 and 496 nm [46–48]. The peak at 456 nm is attributed to oxygen vacancies [49]. The low PL intensity indicates the decrease of recombination rate [47, 50, 51].

Concerning the surface properties of Zr/TiO_2 oxides, the XPS was performed. The Zirconium binding energies (BEs) of Zr 3p at 332.2 and 346 eV and of Zr 3d5/2 at 181.4 eV confirm the presence of Zr in the form of ZrO_2, not metallic Zr (Supporting material, Fig. S1). The Ti is present in the form of TiO_2 and substochiometric Ti oxides. The BEs of Ti2p3/2 at 458.3 eV and Ti2p1/2 at 463.8 eV (Supporting material, Fig. S2) and corresponding O1s at ~530 eV (Supporting material, Fig. S3) corroborate to the presence of TiO_2. The shift in Ti2p3/2 to 455.5 eV and Ti2p1/2 at 461.3 eV corresponds to Ti^{2+} presented in a low amount (Table 3). The shoulder at the left side at 530 eV (towards higher energies) can be attributed to lattice oxygen and oxygen vacancies [52]. The elementary composition determined by XPS is summarized in Table 3. The amount of hydroxyl groups is decreased at decreased Zr content, although the differences are minor.

Concerning the Zr/Ti atomic ratio, XPS determined significantly higher Zr/Ti ratios than SEM-EDS (Table 4). Surprisingly, the surface Zr/Ti atomic ratios determined by XPS also markedly exceeded the real total Zr/Ti atomic ratios determined by XRF. This can be attributed to the fact that XPS analyzes the surface to the depth <10 nm, while SEM-EDS analyzes to the depth of 1–3 µm. Overall, the Zr/Ti atomic ratios determined by SEM-EDS as well as XPS rise. SEM-EDS-determined Zr/Ti atomic ratios indicate that increasing Zr loading leads to Zr/TiO_2 with Zr^{4+} present probably in the form of amorphous ZrO_2 concentrated in the 1–3 µm depth/surface layer of TiO_2. However, for 0.5 and 2 mol.% Zr, the Zr/Ti atomic ratios represent approximately 50–70% of the total Zr/Ti atomic ratios, and for 7.5 mol.% Zr, the Zr/Ti atomic ratio equals to the total Zr/Ti atomic ratio (Table 4).

From SEM-EDS photographs, it is also evident that the morphology of individual Zr/TiO_2 differs (Fig. 6). While 0.5 and 2 mol.% Zr/TiO_2 show small regular spherical aggregates of nanocrystallites <1 µm size, 7.5 mol.% Zr/TiO_2 shows irregular aggregates of nanocrystallites of different sizes with sharp edges. The surface distribution of individual elements (O, Ti, Zr) in photocatalysts seems to be regular (Supporting Material, Figs. S4 and S5).

3.2 Photocatalytic results

The photocatalytic activity was tested on decomposition of AO7. The photoactivity of 0.5 mol.% Zr/TiO_2, 1 mol.% Zr/TiO_2 and 5 mol.% Zr/TiO_2 was comparable (Fig. 7). The 7.5 mol.% Zr/TiO_2 showed the lowest photoactivity. The highest photoactivity was determined for 2 mol.% Zr/TiO_2. The conversions after 3 h and 8 h of irradiation and rate

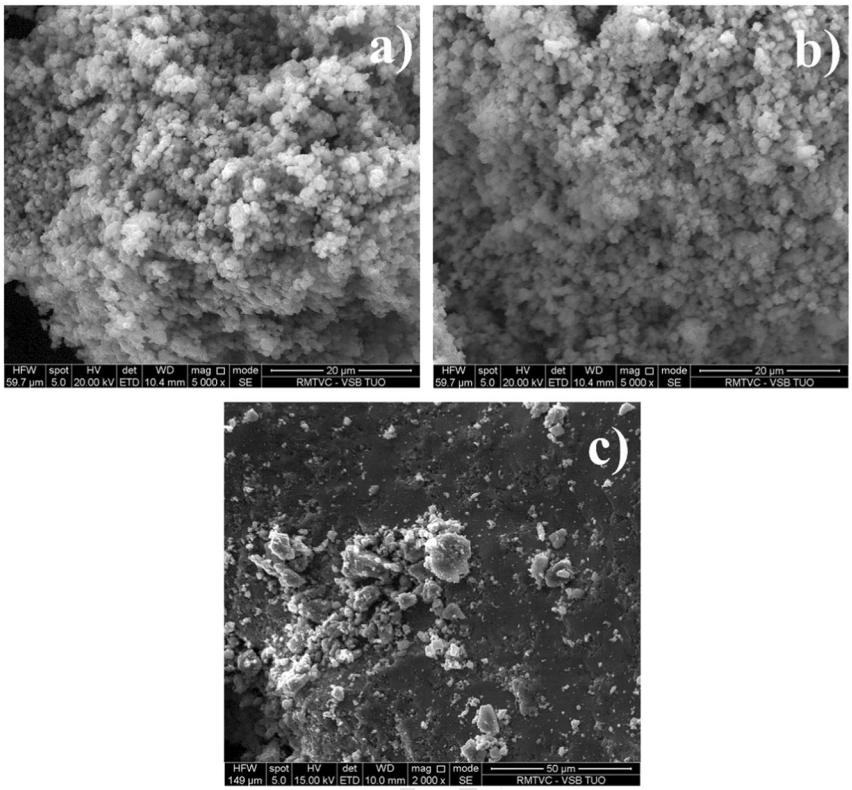

Fig. 6 Scanning electron microscope–energy-dispersive spectrometer (SEM-EDS) photographs of **a** 0.5 mol.% Zr/TiO_2, **b** 2 mol.% Zr/TiO_2 and **c** 7.5 mol.% Zr/TiO_2

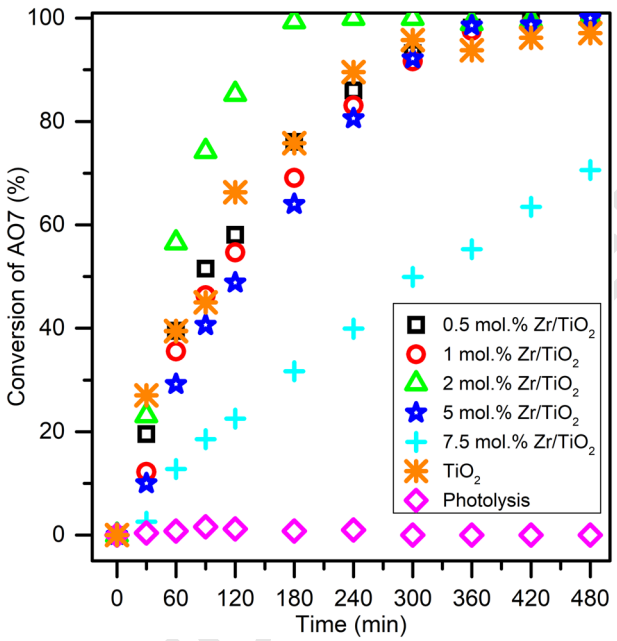

Fig. 7 Time dependencies of AO7 conversion for Zr/TiO_2 oxides

constants are summarized in Table 5. Although 2 mol.% Zr/TiO_2 showed the highest values of k, 0.01431/min, and AO7 conversion of 99% after only 3 h, the TiO_2 Degussa P25 remains unsurpassed (Table 5). All other investigated oxides showed one order lower rate constants than 2 mol.% Zr/TiO_2.

Table 5 Conversions of AO7 after 3 and 8 h of irradiation and reaction rate constants for investigated oxides

Material	X_{AO7} (3h) (%)	X_{AO7} (8h) (%)	$k{\cdot}10^3$ (/min)
0.5 mol.% Zr/TiO_2	76	100	9.14 ± 0.34
1 mol.% Zr/TiO_2	69	100	9.43 ± 0.42
2 mol.% Zr/TiO_2	99	100	14.31 ± 1.28
5 mol.% Zr/TiO_2	64	100	9.40 ± 0.55
7.5 mol.% Zr/TiO_2	32	71	2.36 ± 0.05
TiO_2 [36]	76	97	8. 13 ± 0.33
TiO_2 Degussa P25	100[a]	100	24.88 ± 2.45

[a]After 2 h

3.3 Discussion on the microstructure/defects/morphology–photoactivity correlation

With respect to comparison of structure and optical properties and photocurrent measurements of prepared Zr/TiO_2 photocatalysts with 0.5–7.5 mol.% Zr, it can be said that there are negligible differences between the materials. The phase composition indicates the presence of TiO_2 anatase in all Zr/TiO_2 photocatalysts. Based on the change of anatase lattice parameters, it can be assumed that Zirconium was incorporated to the TiO_2 anatase crystal structure. The Zr dopation resulted in increased anatase crystallite size (from ~13 to ~16 nm) which is in good agreement with the results from our previous study [36]. Correspondingly, the specific

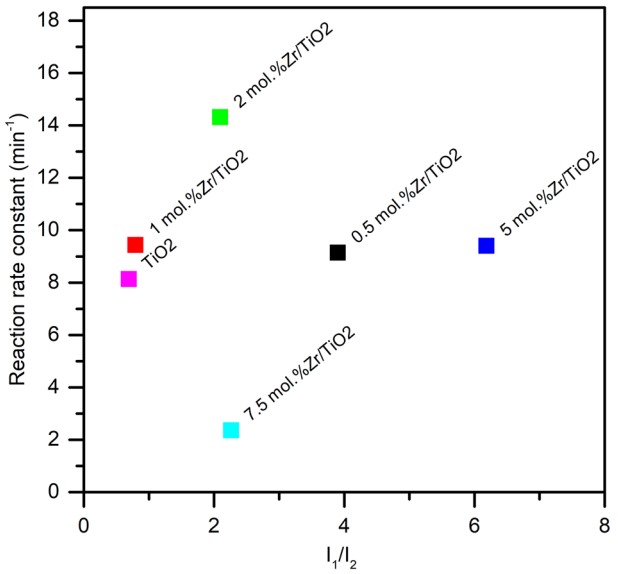

Fig. 8 The correlation between the type of defect and their relative amount, I_1/I_2, and the reaction rate constant, k, of investigated Zr/TiO_2 in AO7 photodegradation

surface area of Zr/TiO_2 photocatalysts decreased (from ~100 to ~83 m^2/g) with the increasing Zr content. The increased concentration of oxygen defects had a positive effect on the photocurrent generation which stems from increased recombination time as it can be seen from the photocurrent and PL results of 0.5 mol.% Zr/TiO_2, 5 mol.% Zr/TiO_2 and 7.5 mol.% Zr/TiO_2. This is in good agreement with the results from ref. [37] and confirms that although the photocatalyst may generate large number of excitons and have increased recombination time due to the presence of defects, this does not secure a good photocatalytic performance (0.5 mol.% Zr/TiO_2 showed the highest photocurrent response but the highest photodegradation rate of AO7 was achieved with 2 mol.% Zr/TiO_2). Several mechanisms take place in photocatalyst, from generation of exciton pair, transport of the electrons and holes to the surface, adsorption of the pollutant onto the photocatalyst surface, formation of reactive species on the photocatalyst, to diffusion of the degraded products, etc. All of these mechanisms are rooted in material properties such as specific surface area, surface charge, phase composition, crystallite morphology and size, band gap and charge carriers' recombination, defects on surface or in crystal lattice, material morphology, etc.

In order to understand the influence of different Zr loading in TiO_2 on the type and amount of defects and their role/effect in the Zr/TiO_2 photocatalytic activity in AO7 photodegradation, the correlation in Fig. 8 is shown. Namely, in Fig. 8 the correlation between the relative ratio of defects of two types, I_1/I_2, (I_1 is the area of peak with maximum at 428 nm, I_2 is the area of peak with maximum at 557 nm in emission spectra, Fig. 5) and the reaction rate constant, k, of individual Zr/TiO_2 is depicted. It is worth mentioning that TiO_2 Degussa P25 was not included in this correlation since it possesses significantly different phase composition (80 wt.% anatase + 20 wt.% rutile) than investigated Zr/TiO_2 (anatase) and, thus, its emission spectrum is different from that of other investigated Zr/TiO_2 (Fig. 5). The results for parent TiO_2 should also be taken into account with caution since it is anatase–brookite mixture (Table 2). The correlation was created since it was reported that the certain type of defects/oxygen vacancies can affect the photocatalytic activity of catalysts [53]. However, from Fig. 8 it is evident that in the case of Zr/TiO_2 with low Zr loadings, any certain type of defect does not crucially influence the Zr/TiO_2 photocatalytic activity, and there exists the optimal Zr loading of 2 mol.%. Since in the cases of 2 and 7.5 mol.% Zr in TiO_2 there are comparable types of defects and their relative amounts, but photocatalysts show significantly different photocatalytic activity corresponding to significantly different kinetic rate constants, it is obvious that there exists some material aspect/property which plays the crucial role in photoactivity, but stays still unrevealed.

Considering the fact that (i) 7.5 mol.% of Zr in TiO_2 corresponds to high content of ~10 wt.% of ZrO_2 besides TiO_2, however, XRD did not reveal any crystalline polymorph of ZrO_2 and (ii) due to larger ionic radius of Zr^{4+} compared to Ti^{4+} the saturation of TiO_2 anatase crystal lattice by Zr^{4+} may be expected at low atomic % of Zr, it may be supposed the Zr^{4+} is present as ZrO_2 amorphous phase/clusters in 7.5 mol.% Zr/TiO_2. This amorphous phase covers/is part of agregated TiO_2 anatase nanocrystallite surface. This result corresponds to SEM-EDS observations when for 7.5 mol.% Zr/TiO_2 the SEM-EDS determined Zr/Ti atomic ratio to the total Zr/Ti ratio determined by XRF, proving Zr^{4+} present in the 1–3 μm surface layer of TiO_2 nanocrystallite agregates. The present amorphous ZrO_2 may cover the anatase nanocyrstallites surface, and thus the anatase surface is shielded against UV light. This material feature is probably a consequence of the synthesis method. The colloid solution of mixture of two precursors—titanyl sulfate and zirconium oxynitrate—starts to precipitate after reaching ~90 °C temperature. It is not clear if the hydrolysis of the precursors (precipitation) is simultaneous or it occurs separately. It is obvious that for 0.5–5 mol.% of Zr in TiO_2, the photocatalytic activity of Zr/TiO_2 is comparable with the exception of 2 mol.% of Zr in TiO_2 when the significantly higher photoactivity was reached. This indicates the existence of the optimal Zr loading in TiO_2 to be 2 mol.%.

4 Conclusion

Zr/TiO_2 anatase photocatalysts with low Zr loading (0.5–7.5 mol.%) were prepared via colloid solution precipitation by thermal hydrolysis and using pressurized hot water crystallization, and their photocatalytic activity was investigated in AO7 photodegradation at 365 nm UV light. The photocatalyst activity decreased as follows: 2 mol.% Zr/TiO_2 > TiO_2 ~0.5 mol.% Zr/TiO_2 ~1 mol.% Zr/TiO_2 ~5 mol.% Zr/TiO_2 > 7.5 mol.% Zr/TiO_2. The lowest photocatalytic activity of 7.5 mol.% Zr/TiO_2 can be attributed to the presence of amorphous ZrO_2 dominantly in the surface layer (~1–3 μm depth) of TiO_2 anatase nanocrystallite agregates which changed the morphology of TiO_2 nanocrystallite aggregates and shielded the anatase nanocrystallite surface. It was revealed that the type and amount of defects (e.g., oxygen vacancies, lattice defects) do not affect the photoactivity of Zr/TiO_2 in AO7 photodegradation. The addition of Zr to TiO_2 changes significantly the morphology of the photocatalyst and affects the location of the formed amorphous ZrO_2. The optimal zirconium loading in TiO_2 was determined to be 2 mol.%. Against all expectations, the photoelectrochemical measurements did not offer a satisfactory explanation of different Zr/TiO_2 photoactivity.

Acknowledgements This work was supported from ERDF "Institute of Environmental Technology – Excellent Research" (No. CZ.02.1.01/0.0/0.0/15_019/0000853). Experimental results were accomplished using Large Research Infrastructure ENREGAT supported by the Ministry of Education, Youth and Sports of the Czech Republic under project No. LM2018098. The financial support of the Grant Agency of the Czech Republic (project No. 14-23274S) is also gratefully acknowledged. XPS measurements were carried out with the equipment purchased thanks to the financial support of the NanoEnviCZ supported by the Ministry of Education, Youth and Sports of the Czech Republic under project No. LM2015073. The authors also thank Dr. Martin Reli from IET VŠB-TUO for his guidance in photoelectrochemical measurements and advices with spectra interpretation.

References

1. Kyoto Protocol to the United Nations Framework Convention on Climate Change (1997). Kyoto
2. Coronado JM, Fresno F, Hernández-Alonso MD, Portanela R (2013) Design of advanced photocatalytic materials for energy and environmental applications. Springer, London
3. Nakata K, Fujishima A (2012) TiO_2 photocatalysis: design and applications. J Photochem Photobiol C Photochem Rev 13 (3):169–189
4. Ong CB, Ng LY, Mohammad AW (2018) A review of ZnO nanoparticles as solar photocatalysts: synthesis, mechanisms and applications. Renew Sustain Energy Rev 81:536–551
5. Harandi D, Ahmadi H, Achachluei MM (2016) Comparison of TiO_2 and ZnO nanoparticles for the improvement of consolidated wood with polyvinyl butyral against white rot. Int Biodeterior Biodegrad 108:142–148
6. Znaidi L (2010) Sol-gel-deposited ZnO thin films: a review. Mater Sci Eng B Adv 174(1-3):18–30
7. Khedr TM, El-sheikh SM, Hakki A, Ismail AA (2017) Highly active non-metals doped mixed-phase TiO_2 for photocatalytic oxidation of ibuprofen under visible light. J Photochem Photobiol A Chem 346:530–540
8. Xing Z, Zhang J, Cui J, Yin J, Zhao T, Kuang J, Xiu Z, Wan N, Zhou W (2018) Recent advances in floating TiO_2 -based photocatalysts for environmental application. Appl Catal B Environ 225:452–467
9. Mahy JG, Lambert SD, Léonard GLM, Zubiaur A, Olu P-Y, Mahmoud A, Boschini F, Heinrichs B (2016) Towards a large scale aqueous sol-gel synthesis of doped TiO_2: study of various metallic dopings for the photocatalytic degradation of p-nitrophenol. J Photochem Photobiol 329:189–202
10. Wen J, Xie J, Chen X, Li X (2017) A review on g-C_3N_4 -based photocatalysts. Appl Surf Sci 391:72–123
11. Kharlamov A, Bondarenko M, Kharlamova G, Gubareni N (2016) Features of the synthesis of carbon nitride oxide (g-C_3N_4) at urea pyrolysis. Diam Relat Mater 66:16–22
12. Xiao H, Wang W, Liu G, Chen Z, Lv K, Zhu J (2015) Photocatalytic performances of g-C_3N_4 based catalysts for RhB degradation: effect of preparation conditions. Appl Surf Sci 358:313–318
13. Ma J, Wang C, He H (2016) Enhanced photocatalytic oxidation of NO over g-C_3N_4 -TiO_2 under UV and visible light. Appl Catal B Environ 184:28–34
14. Zhang J, Xu LJ, Zhu ZQ, Liu QJ (2015) Synthesis and properties of (Yb, N)-TiO_2 photocatalyst for degradation of methylene blue (MB) under visible light irradiation. Mater Res Bull 70:358–364
15. Naraginti S, Thejaswini TVL, Prabhakaran D, Sivakumar A, Satyanarayana VSV, Prasad ASA (2015) Enhanced photocatalytic activity of Sr and Ag co-doped TiO_2 nanoparticles for the degradation of Direct Green-6 and Reactive Blue-160 under UV & visible light. Spectrochim Acta A 149:571–579
16. Matějová L, Šihor M, Brunátová T, Ambrožová N, Reli M, Čapek L, Obalová L, Kočí K (2015) Microstructure-performance study of cerium-doped TiO_2 prepared by using pressurized fluids in photocatalytic mitigation of N_2O Res Chem Intermed 41:9217–9231
17. Jiang H, Gomez-Abal RI, Rinke P, Scheffler M (2010) Electronic band structure of zirconia and hafnia polymorphs from the GW perspective Phys Rev B 81:085119
18. Kambur A, Pozan GS, Boz I (2012) Preparation, characterization and photocatalytic activity of TiO_2-ZrO_2 binary oxide nanoparticles. Appl Catal B Environ 115:149–158
19. Lukáč J, Klementová M, Bezdička P, Bakardjieva S, Šubrt J, Szatmáry L, Bastl Z, Jirkovský J (2007) Influence of Zr as TiO_2 doping ion on photocatalytic degradation of 4-chlorophenol. Appl Catal B Environ 74(1-2):83–91
20. Matějová L, Kočí K, Reli M, Čapek L, Matějka V, Šolcová O, Obalová L (2013) On sol-gel derived Au-enriched TiO_2 and TiO_2-ZrO_2 photocatalysts and their investigation in photocatalytic reduction of carbon dioxide. Appl Surf Sci 285:688–696
21. Zou H, Lin YS (2004) Structural and surface chemical properties of sol-gel derived TiO_2-ZrO_2 oxides. Appl Catal A Gen 265 (1):35–42
22. Choina J, Fischer C, Flechsig GU, Kosslick H, Tuan VA, Tuyen ND, Tuyen NA, Schulz A (2014) Photocatalytic properties of Zr-doped titania in the degradation of the pharmaceutical ibuprofen. J Photoch Photobio A 274:108–116
23. Gao BF, Lim TM, Subagio DP, Lim TT (2010) Zr-doped TiO_2 for enhanced photocatalytic degradation of bisphenol A. Appl Catal A Gen 375(1):107–115
24. Inturi SNR, Boningari T, Suidan M, Smirniotis PG (2014) Visible-light-induced photodegradation of gas phase acetonitrile using aerosol-made transition metal (V, Cr, Fe, Co, Mn, Mo, Ni, Cu, Y, Ce, and Zr) doped TiO_2. Appl Catal B Environ 144:333–342
25. Naraginti S, Stephen FB, Radhakrishnan A, Sivakumar A (2015) Zirconium and silver co-doped TiO_2 nanoparticles as visible light

catalyst for reduction of 4-nitrophenol, degradation of methyl orange and methylene blue. Spectrochim Acta A 135:814–819

26. Mattsson A, Lejon C, Štengl V, Bakardjieva S, Opluštil F, Andersson PO, Österlund L (2009) Photodegradation of DMMP and CEES on zirconium doped titania nanoparticles. Appl Catal B Environ 92(3-4):401–410
27. Mattsson A, Lejon C, Bakardjieva S, Štengl V, Osterlund L (2013) Characterisation, phase stability and surface chemical properties of photocatalytic active Zr and Y co-doped anatase TiO_2 nanoparticles. J Solid State Chem 199:212–223
28. Cha JA, An SH, Jang HD, Kim CS, Song DK, Kim TO (2012) Synthesis and photocatalytic activity of N-doped TiO_2/ZrO_2 visible-light photocatalysts. Adv Powder Technol 23(6):717–723
29. Feng HJ, Zhang MH, Yu LYE (2012) Hydrothermal synthesis and photocatalytic performance of metal-ions doped TiO_2. Appl Catal A Gen 413:238–244
30. Tian G, Pan K, Fu H, Jing L, Zhou W (2009) Enhanced photocatalytic activity of S-doped TiO_2-ZrO_2 nanoparticles under visible-light irradiation. J Hazard Mater 166(2-3):939–944
31. Kim CS, Shin JW, An SH, Jang HD, Kim TO (2012) Photodegradation of volatile organic compounds using zirconium-doped TiO_2/SiO_2 visible light photocatalysts. Chem Eng J 204:40–47
32. McManamon C, Holmes JD, Morris MA (2011) Improved photocatalytic degradation rates of phenol achieved using novel porous ZrO_2-doped TiO_2 nanoparticulate powders. J Hazard Mater 193:120–127
33. Fresno F, Hernandez-Alonso MD, Tudela D, Coronado JM, Soria J (2008) Photocatalytic degradation of toluene over doped and coupled $(Ti,M)O_2$ (M = Sn or Zr) nanocrystalline oxides: influence of the heteroatom distribution on deactivation. Appl Catal B Environ 84(3-4):598–606
34. Das M, Bhattacharyya KG (2013) Oxidative degradation of orange II dye in water with raw and acid-treated ZnO, and MnO_2 CLEAN Soil Air Water 41:984–991
35. Konstantinou IK, Albanis TA (2004) TiO_2-assisted photocatalytic degradation of azo dyes in aqueous solution: kinetic and mechanistic investigations - a review. Appl Catal B Environ 49(1):1–14
36. Lang J, Matějová L, Troppová I, Čapek L, Endres J, Daniš S (2017) Novel synthesis of $Zr_xTi_{1-x}O_n$ mixed oxides using titanyl sulphate and pressurized hot and supercritical fluids, and their photocatalytic comparison with sol-gel prepared equivalents. Mater Res Bull 95:95–103
37. Lang J, Matějová L, Matěj Z, Čapek L, Svoboda L (2018) Crystallization of $Zr_{0.1}Ti_{0.9}O_n$ mixed oxide by pressurized hot water and its effect on microstructural properties and photoactivity J Supercrit Fluid 141:39–48
38. Matějová L, Polách L, Lang J, Šihor M, Reli M, Brunátová T, Daniš S, Peikertová P, Troppová I, Kočí K (2017) Novel TiO_2 prepared from titanyl sulphate by using pressurized water processing and its photocatalytic activity evaluation. Mater Res Bull 95:30–46
39. Matěj Z, Kužel R, Nichtová L (2010) XRD total pattern fitting applied to study of microstructure of TiO_2 films. Powder Diffr 25 (2):125–131
40. Zdeněk M (2014) Refining bimodal microstructure of materials with MSTRUCT. Powder Diffr 29(S2):35–41
41. Gregg SJ, Sing KSW (1982) Adsorption, surface area and porosity, 2nd edn. Academic Press, New York
42. Brunauer S, Emmett PH, Teller E (1938) Adsorption of gases in multimolecular layers. J Am Chem Soc 60:309–319
43. Shannon RD (1976) Revised effective ionic-radii and systematic studies of interatomic distances in halides and chalcogenides. Acta Crystallogr A 32(Sep1):751–767
44. Li Z, Wang W, Greenham NC, McNeill CR (2014) Influence of nanoparticle shape on charge transport and recombination in polymer/nanocrystal solar cells. Phys Chem Chem Phys 16 (47):25684–25693
45. Tang H, Prasad K, Sanjinès R, Schmid PE, Lévy F (1994) Electrical and optical properties of Ti_O2 anatase thin films. J Appl Phys 75(4):2042–2047
46. Abazović ND, Čomor MI, Dramićanin MD, Jovanović DJ, Ahrenkiel SP, Nedeljković JM (2006) Photoluminescence of anatase and rutile Ti_O2 particles. J Phys Chem B 110(50):25366–25370
47. Sabry RS, Al-Haidarie YK, Kudhier AM (2016) Synthesis and photocatalytic activity of TiO_2 nanoparticles prepared by sol–gel method. J Sol Gel Sci Technol 78(2):299–306
48. Liu B, Wen L, Zhao X (2007) The photoluminescence spectroscopic study of anatase TiO_2 prepared by magnetron sputtering. Mater Chem Phys 106(2-3):350–353
49. Kernazhitsky L, Shymanovska V, Gavrilko T, Naumov V, Fedorenko L, Kshnyakin V, Baran J (2014) Laser-excited excitonic luminescence of nanocrystalline TiO_2 powder. Ukr J Phys 59(3):246–253
50. Suisalu A, Aarik J, Mndar H, Sildos I (1998) Spectroscopic study of nanocrystalline TiO_2 thin films grown by atomic layer deposition. Thin Solid Films 336(1-2):295–298
51. Anpo M, Kamat PV (eds) (2010) Photoluminescence spectroscopic studies on TiO_2 photocatalyst. Springer, New York
52. Fu C, Gong Y, Wu Y, Liu J, Zhang Z, Li C, Niu L (2016) Photocatalytic enhancement of TiO_2 by B and Zr co-doping and modulation of microstructure. Appl Surf Sci 379:83–90
53. Reli M, Edelmannová M, Šihor M, Praus P, Svoboda L, Mamulová KK, Otoupalíková H, Čapek L, Hospodková A, Obalová L, Kočí K (2015) Photocatalytic H_2 generation from aqueous ammonia solution using ZnO photocatalysts prepared by different methods. Int J Hydrog Energy 40(27):8530–8538

Journal : **10971**
Article : **4956**

Springer
the language of science

Author Query Form

Please ensure you fill out your response to the queries raised below and return this form along with your corrections

Dear Author

During the process of typesetting your article, the following queries have arisen. Please check your typeset proof carefully against the queries listed below and mark the necessary changes either directly on the proof/online grid or in the 'Author's response' area provided below

Queries	Details Required	Author's Response
AQ1	Please confirm that the edit to the sentence 'The anthropogenic….' preserves the originally intended meaning.	
AQ2	Per journal style, please provide Highlights section.	
AQ3	Please confirm that the edits to the sentence 'The Pt wire served as….' preserve the originally intended meaning.	
AQ4	Please describe panels 'a' and 'b' in Figure 2 legend.	
AQ5	Please confirm the change of closets to closest is correct in the sentence 'The Fig. 4b shows....'.	
AQ6	Please confirm that the edits to the sentence 'Such a result….' preserve the originally intended meaning.	
AQ7	References 50 and 51 were not cited in the text. Hence they have been cited at the end of the sentence 'The low PL.....'. Is it ok?	
AQ8	Please confirm that the edits to the sentence 'This can be attributed….' preserve the originally intended meaning.	
AQ9	Please check the sentence 'Considering the fact ….' for clarity.	
AQ10	Please check the sentence 'The photocatalyst activity decreased….' for clarity. The usage of punctuation is not clear.	
AQ11	Please provide Conflict Of Interest Statement.	
AQ12	Please provide the author names and publisher name in reference 1.	
AQ13	Please check and confirm the edits are correct in reference 51.	